Sixth International Symposium on Turbulence and Shear Flow Phenomena
Seoul, Korea, 22-24 June 2009

DIAGNOSTICS AND CONTROL OF LARGE-SCALE STRUCTURES IN SWIRLING PREMIXED FLAMES

Sergey V. Alekseenko[1,2], Vladimir M. Dulin[1], Yuriy S. Kozorezov[1], Dmitriy M. Markovich[1,2]*, Sergey I. Shtork[1]
1: Institute of Thermophysics, Siberian Branch of RAS,
1 Lavrentyev avenue, Novosibirsk, 630090, Russia
*: dmark@itp.nsc.ru

2: Department of Physics,
Novosibirsk State University,
2 Pirogova street, 630090, Russia

ABSTRACT

The present work is devoted to the experimental study of the flow structure of premixed swirling jet flames at various combustion regimes. A stereo PIV technique combined with a pressure probe was used for the investigation of the role of large-scale vortices in turbulent structure of the flames. Instantaneous velocity and vorticity fields were estimated, as well as the spatial distributions of the mean velocity and turbulent kinetic energy components. To determine a shape and location of the flame front, chemiluminescence images captured by an ICCD camera were used. The analysis of the results is aimed for the efficiency of active (by applying an acoustic forcing) and passive (by introducing a swirl) ways to control properties of large-scale vortices strongly affecting the combustion in turbulent flame.

INTRODUCTION

Presently, starting from the works of Harris et al. (1949), the structure and stability of a non-swirling (Bunsen) hydrocarbon jet flame, is comprehensively studied for a wide range of inlet velocities and fuel-air ratios. Generally, the flame can be stabilized between two limiting values of the flow rate. The lower value is a flashback limit, below which the flame can't anchor itself to the lip of the burner rim and flashes back inside the burner. The upper value is a blow-off limit, for which the flame can't be longer stabilized in the region of interest and it is carried away by the upstream flow. Besides, when the flow rate exceeds a certain value, but prior to the blow-off event, a 'lifted' combustion regime can be observed. In this case, the flame abruptly becomes detached from the burner lip and remains stably positioned at a certain distance from the burner.

In practice, modern combustion devices utilize lean premixed flames to achieve a low level of NOx emissions. However, lean premixed flames are rather sensitive to instabilities induced by various sources, including flame unsteadiness and blow-off (Lieuwen et al., 2001). Thus, the application of a relatively strong swirl with corresponding appearance of a vortex breakdown with a recirculation zone is usually used for the flame stabilization. The vortex precession itself and intensive turbulent fluctuations, typical for the vortex breakdown, increase the flame stabilization via a high turbulent mixing rate of the fresh and burnt gases in the back-flow region. This allows to maintain the combustion at rather lean conditions. However, even for the isothermal swirling jets, substantially different flow regimes can be observed, depending on the swirl rate and on the manner in which the swirl is applied (Billant et al., 1998; Liang and Maxworthy, 2005; among others). It is widely acknowledged by many authors that Kelvin–Helmholtz instability leading to vortex rings formation, dominates in the shear layer of non-swirling and weakly swirling jets. For a high enough swirl rate (but before appearance of pronounced vortex breakdown) strong helical waves were usually observed in the mixing layer of the jet. Further increase of a swirl rate leads to the initiation of a vortex breakdown, which is known to have different states (Alekseenko et al., 2007): spiral, bubble, or conical, where the last two can be either symmetric or asymmetric (e.g. Billant et al., 1998). Obviously, the presence of combustion makes the structure of the swirling jets much more complex. Observations of different authors show that for the turbulent swirling flames a great variety of the combustion regimes can exist resulting from such effects, as thermal expansion (strong buoyancy effect on a swirling jet was reported by Mourtazin and Cohen, 2007), etc. In particular, Schneider et al. (2005) reported that the presence of combustion can suppress the vortex precession in the swirling jet flow.

For the turbulent premixed combustion, depending on the ratio of characteristic scales of turbulence and flame, various effects can take place. Velocity fluctuations tend to increase propagation speed of the flame front, while thermal expansion effect suppresses the turbulence in the gas passing thru the flame layer (e.g. Treurniet et al., 2006). Besides, large-scale vortices interacting with the flame front result its intensive fluctuations and, consequently, fluctuations of the heat-release that leads to increase of acoustic noise (Schuller et al., 2002). Thus, such interaction can lead to harmful resonance effects in confined combustion facilities. At the same time, pressure waves form the flame/vortex interactions can result intensification of large-scale vortices in shear flows. In particular, the external acoustic forcing is able to significantly increase

combustion rate in non-swirling jet flames (see Yoshida et al., 2001). Similarly to the non-swirling jets, external forcing of inlet velocity can be used to control the development of large-scale vortices and thus the turbulent mixing in weakly (Gallaire et al., 2004) and even in strongly (Alekseenko et al., 2008) swirling jets.

Presently, particle image velocimetry (PIV) has become a commonly used technique for the velocity measurements in isothermal flows. Significant advantage of PIV is that it provides the measurement of instantaneous velocity fields, and thus, allows to study the spatial structure of vortices emerging in turbulent flows. Today, there is several papers presented in literature which are devoted to the experimental study of the flows with combustion by using PIV. In particular, the aspects of PIV application to turbulent flames were deeply described in Stella et al. (2001). It was shown that for laboratory-size flames, inaccuracy resulting from refractive index variation is quite small in terms of laser sheet deflection and image deformation. Also it was shown that Al_2O_3 particles, surviving the flame, are able to follow the flow properly, except for flame front regions and small-scale velocity fluctuations because of a large relaxation time of the particles.

In this context, the present paper is aimed for the stereo PIV study of the large-scale vortices role in the flow structure and combustion regimes of turbulent swirling flames.

EXPERIMENTAL SETUP AND APPARATUS

The measurements were performed in a combustion rig (Figure 1a) consisted of a burner, air fan, plenum chamber, flow seeding device, premixing chamber and section for the air and fuel (propane) flowrate control. The experiments were performed at atmospheric pressure. During the study, Re_{air} number (based on the nozzle exit diameter d and flowrate velocity of the air and on viscosity of the air) was varied from 500 to 8,000. The equivalence ratio Φ of air-propane mixture was varied from 0.5 to 10. In order to provide PIV measurements of the instantaneous velocity, the flow was seeded by oxide aluminium particles with the average diameter of 5 μm. For external acoustic forcing of the flow, a system consisting of four loud speakers, parallel connected to an amplifier, function generator and electric power meter, was used. The normalized (by nozzle exit diameter d and the mean flowrate velocity U_0 of the mixture) forcing frequency, i.e. the Strouhal number, was varied from 0.1 to 3. The burner represented a profiled contraction nozzle with the same geometry as in the isothermal water jet experiments by Alekseenko et al. (2008). The contraction nozzle was designed to provide a 'top-hat' velocity distribution at the nozzle exit for the non-swirling flow. The nozzle exit diameter d was 15 mm, and the area contraction rate was 18.8. For organization of the flows with swirl, smoothing grids in a plenum chamber of the nozzle were replaced by a swirl generator as shown in Fig. 1b. The definition of the swirl rate was based on the swirler geometry according to Gupta et al. (1984):

$$S = \frac{2}{3}\left(\frac{1-(d_1/d_2)^3}{1-(d_1/d_2)^2}\right)\tan(\varphi) \qquad (1)$$

Here, $d_1 = 7$ mm is the diameter of a centerbody supporting the blades, $d_2 = 27$ mm is the external diameter of the swirler, and φ is the blades' inclination angle. For the swirler with $\varphi = 55°$, used in the experiments, the swirl rate S was equal to 1.0. The definition of the swirl rate based on the swirler geometry was used as the reference to the experimental setup case. According to Alekseenko et al. (2008), for the present geometry the swirl rate defined as the ratio of the axial flux of angular momentum to the axial flux of axial momentum was 0.79.

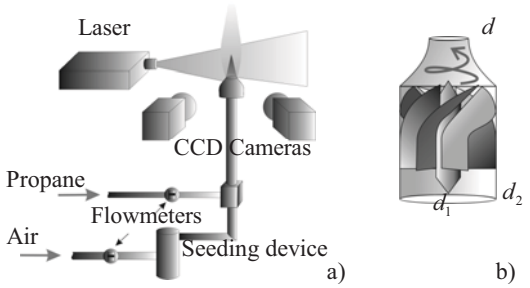

Figure 1. (a) Scheme of combustion rig and measurement system arrangement. (b) Scheme of swirler arrangement.

For the instantaneous velocity measurements a "PIV-IT" Stereo PIV system consisting of a double-cavity Nd:YAG pulsed laser, couple of CCD cameras and a synchronizing processor was used. The cameras were equipped with narrow-bandwidth optical filters admitting emission of the laser (532 nm) and suppressing radiation of the flame. The system was operated by a computer with "ActualFlow" software. Measured images were processed by an iterative cross-correlation algorithm with an image deformation and with a final interrogation area size of 32×32 pixels and 50% overlap. Due to non-uniform seeding on the flow, the used cross-correlation algorithm was modified to account for the number of the tracer particles present in each interrogation area. Calculated instantaneous velocity fields were validated by using a signal-to-noise criterion for cross-correlation maxima and by an adaptive median filter proposed in Westerweel and Scarano (2005). Before the stereo reconstruction, the identified "outliers" were removed and the "holes" were interpolated by using a 3rd-order 3×3 linear interpolation filter. Stereo calibration was performed by using a plane calibration target and a 3rd-order polynomial transform. Additionally, to minimize stereo calibration error connected with possible misalignment of the laser sheet and target plane, an iterative correction procedure (Coudert and Schon, 2001) was applied. All the measurements were performed in a central plane of the jet/flame. For each combustion regime 2,500 instantaneous three-component velocity fields were measured.

For analysis of the flame front instantaneous shape, the CH* chemiluminiscence signal was captured by an UV sensitive ICCD camera equipped with a band-pass optical filter (430±5 nm). The exposure duration was about 100 μs that is close to the delay between couple of PIV images captured for measurements of the flow velocity.

The instantaneous pressure was measured by a condenser microphone (Behringer ECM8000) with the tip

installed at a radial distance of one meter from the nozzle axis. The acquisition of the microphone signal was performed by an ADC with 2 kHz sampling rate and 16-bits resolution. For the each combustion regime three independent measurements with 10 seconds duration were performed. Besides, to insure that the contribution of noise from the air fan and other sources to the measurements of the pressure fluctuation was small, three series of additional measurements were taken when the flame was externally extinguished.

RESULTS

On the basis of the estimated instantaneous velocity fields, the spatial distributions of the mean velocity and components of turbulent kinetic energy (TKE) were calculated. To investigate spatial structure of the large-scale vortices emerging in the studied flows, a second-order centred difference scheme was used to calculate instantaneous vorticity fields. One should mention that the used scheme is a low-pass derivative filter with the transfer function similar to one of the cross-correlation operation in case of 50% interrogation area overlap. Thus, the distribution of the instantaneous vorticity and velocity shown below corresponds only to large-scale fluctuations (not lesser than 1.1 mm). For the studied combustion regimes the data from the microphone were used to estimate the intensity of pressure fluctuations emitted by the flame. Besides the direct photographs of the combustion regime, the images from the ICCD camera were used to analyse instantaneous shape of the flame front.

Non-swirling flame

Figures 2a and b show the direct image of the flame and CH* chemiluminescence signal, respectively, for the lifted non-swirling jet flame at Φ = 2.0 and Re_{air} = 4,100 (U_0 = 4.6 m/s). From Figure 2a one can observe that the region where the combustion takes place is located at a certain distance from the nozzle. Shown in Figure 2b chemiluminescence image indicates that the shape of the flame is rather similar to that, observed in the study of the lifted jet diffusion flame by Su et al. (2000).

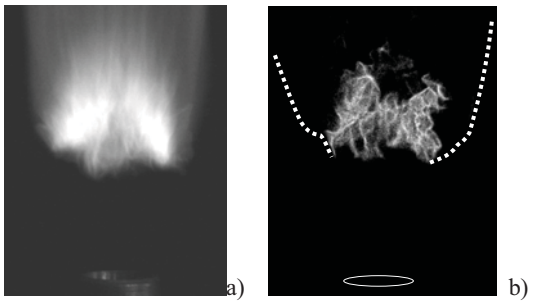

Figure 2. (a) Photograph and (b) CH* chemiluminescence image for a non-swirling lifted jet flame at Φ = 2.0, Re_{air} = 4,100, U_0 = 4.6 m/s.

The flame front location was observed to oscillate around z/d = 1.3 and the oscillations were accompanied with intensive acoustic noise. The r.m.s. value of the pressure fluctuations, measured by the microphone, was $\langle p^2 \rangle^{1/2}$ = 0.29 Pa that corresponds to the sound pressure level (SPL) of 83 dB.

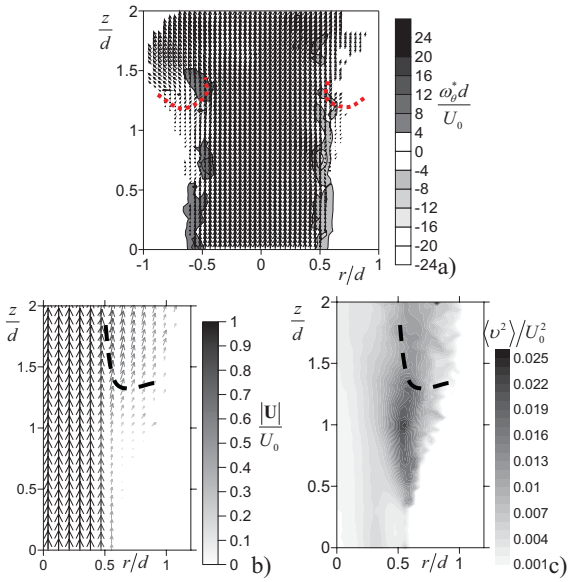

Figure 3. Spatial distribution of the (a) instantaneous velocity and vorticity, (b) mean velocity, (c) radial component of TKE for a lifted non-swirling flame at Φ = 2.0, Re_{air} = 4,100, U_0 = 4.6 m/s.

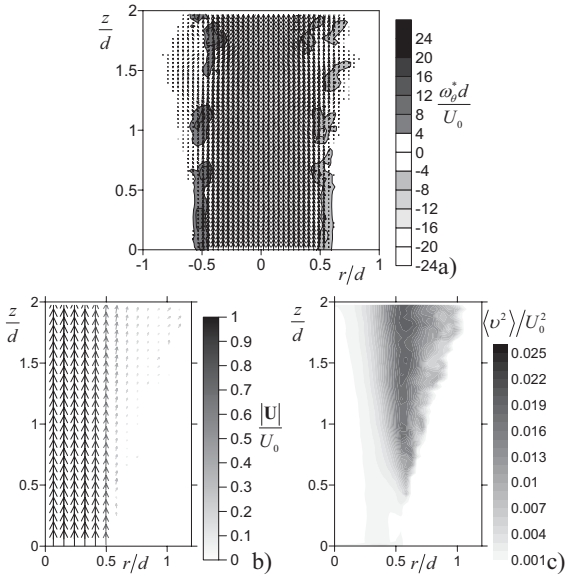

Figure 4. Spatial distribution of the (a) instantaneous velocity and vorticity, (b) mean velocity, (b) radial component of TKE for a non-swirling jet at Re_{air} = 4,100, U_0 = 4.6 m/s..

The intensive pressure fluctuations were considered to be mainly caused by oscillations of the heat release rate due to the variation of the flame surface, caused by the front interaction with the large-scale vortices generated in the isothermal mixing layer of the jet before the lifted flame. Figures 3a and 4a show the examples of the instantaneous velocity fields for the reacting (Φ = 2.2) and isothermal

non-swirling jets, respectively (Re = 4,100). The flame front is schematically shown by the dashed line. Figures 3b,c and 4b,c also present the average velocity fields (each fourth vector is shown) and the radial component of TKE for these flows. By analysing the instantaneous velocity fields for the flows without and with combustion, one can conclude that in the latter case the vortices formed in the shear layer of the jet are more pronounced before the flame front and their magnitude decreases behind it (due to the thermal expansion). The observations on vortices intensity are clearly reflected by the magnitude of TKE components distributions. Besides, a locally great spreading rate was observed on the averaged velocity fields downstream of the flame front.

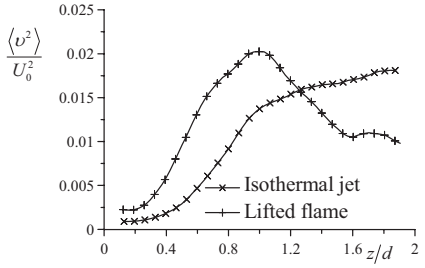

Figure 5. Distributions of the radial component of TKE along the mixing layer ($r/d = 0.55$) of isothermal and reacting non-swirling jets at $\Phi = 2.0$, $\mathrm{Re}_{air} = 4{,}100$, $U_0 = 4.6$ m/s.

Evolution of the radial component of TKE $\langle v^2 \rangle$ along the mixing layer (i.e., $r/d = 0.55$ cross-section) for the lifted jet flame is shown in Figure 5 in comparison with the flow without combustion. For the first case, $\langle v^2 \rangle$ almost linearly decreases in the region $1.0 < z/d < 1.5$, where the flame front effect on the large-scale vortices is highest. In both cases one can clearly observe exponential growth of $\langle v^2 \rangle$ with z in the vicinity of the nozzle. For the flame, the growth rate is about 20% greater than in the isothermal case, and, in general, the difference in the distributions is rather similar to that between the cases of the unforced and forced turbulent jet described in Alekseenko et al. (2008). Thus, the pressure fluctuations, from the interaction of the ring-like vortices with the flame front, act as the acoustic forcing (feed-back) of the isothermal jet shear layer and lead to more intensive development of the consequent vortices. This increases turbulent fluctuations and propagation speed of the flame front. Thus, one can state that the 'lifted' premixed flame is stabilized via the nonlinear feed-back mechanism. This observation is also supported by the acoustics forcing. Figure 6 shows direct photographs of the described above lifted flame without and with external acoustic forcing. The most interesting case is shown, when the forcing at St = 1.73 (as well as at St = 1.3) leads to decrease of the distance between the nozzle and flame front. This can be explained by a more fast growth of turbulent fluctuations in the mixing layer of the jet. There also were several frequencies (e.g. St = 1.95 and 2.5), when the flame front was blown away in several tens of seconds after the acoustic forcing was initiated. This can be explained by the negative effect of the forcing in terms of the vortices generation enhancement.

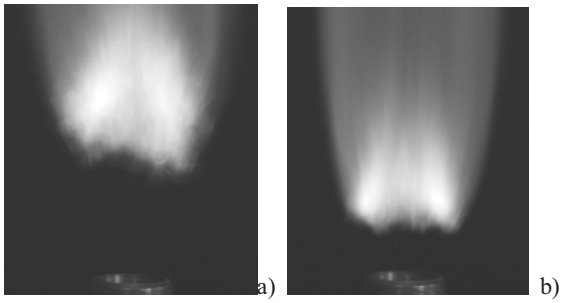

Figure 6. Photographs of an (a) unforced and (b) forced (St = 1.73) non-swirling lifted jet flame at $\Phi = 2.0$, $\mathrm{Re}_{air} = 4{,}100$, $U_0 = 4.6$ m/s.

Swirling flame

The present section describes the results of experimental study of the swirling turbulent flame at relatively high swirl rate ($S = 1.0$). Before describing these results, the present section also addresses to the data of Alekseenko et al. (2008) on the isothermal swirling jet flow (Re = 8,900) at the same nozzle geometry. Figure 7 shows the example of the instantaneous velocity field and the spatial distributions of the mean velocity and radial component of TKE.

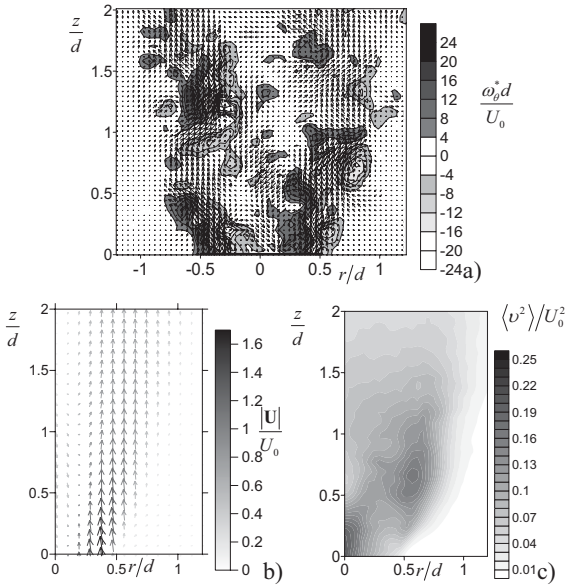

Figure 7. Spatial distribution of the (a) instantaneous velocity and vorticity, (b) mean velocity, (b) radial component of TKE for an isothermal swirling jet at Re = 8,900, $U_0 = 0.52$ m/s.

In the mean velocity field (the colour scale corresponds to the absolute value of the mean velocity vector, i.e., $|\mathbf{U}| = (U^2 + V^2 + W^2)^{1/2}$, while the vector length is proportional to $(U^2 + V^2)^{1/2}$), the presence of a recirculation zone in the initial region of the jet (up to $z/d = 1.8$) can be observed. The mean axial velocity reached the negative minimum value of $U = -0.48U_0$ at $z/d = 0.6$. Analyzing the structure of large-scale vortices in the measurement plane, it was concluded, that among a band of various modes, typical for a turbulent jet, couple of large-scale helical vortices dominate in the jet flow. One vortex is located inside the

recirculation zone, while the other one is located outside, in the outer mixing layer of the jet. The notion about spatial structure of the vortices is based on the results by Liang and Maxworthy (2005), where for a swirling free jet (Re = 1,000, S = 0.9) with vortex breakdown, +1 azimuthal mode, corresponding to a couple of the similar vortices induced by a precession of the vortex core of the jet, was found to be the most powerful. In the present case, the strong precession of the vortex core is also observed in the region of locally high values of $\langle v^2 \rangle$ (that reaches of $0.21 U_0^2$) for $z/d < 0.4$ and $r/d < 0.2$.

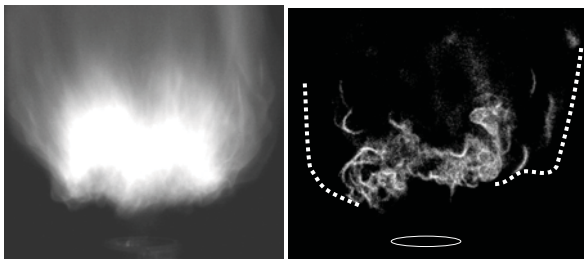

Figure 8. (a) Photograph and (b) CH* chemiluminescence image for a swirling lifted flame at $\Phi = 2.3$, $\mathrm{Re}_{air} = 4{,}100$, $U_0 = 4.7$ m/s.

Figures 8a and b show photograph and CH* chemiluminescence image, respectively, for the lifted swirling jet flame at $\Phi = 2.3$ and Re = 4,100 ($U_0 = 4.7$ m/s). As for the non-swirling lifted flame, intensive oscillation of the combustion zone was observed and the r.m.s. value of pressure fluctuations was $\langle p^2 \rangle^{1/2} = 0.88$ Pa (i.e., 93 dB SPL).

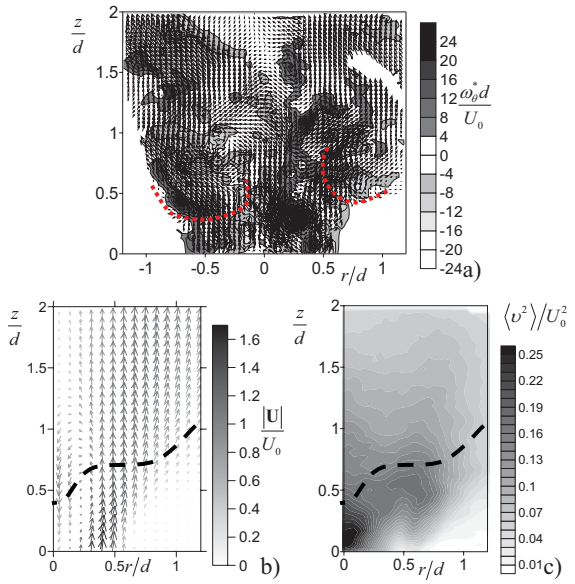

Figure 9. Spatial distribution of the (a) instantaneous velocity and vorticity, (b) mean velocity, (b) radial component of TKE for a lifted swirling flame at $\Phi = 2.3$, $\mathrm{Re}_{air} = 4{,}100$, $U_0 = 4.7$ m/s.

Images of CH* signal indicate that the flame front has much more complex and sufficiently three-dimensional shape than for the non-swirling lifted flame described above. Besides, interaction of the intensive large-scale vortices (which seem to have similar spatial structure as in the isothermal flow) with the flame front resulted in 3 times more intensive pressure fluctuations than for the non-swirling lifted flame. Figure 9 shows the instantaneous velocity fields and the distributions of the mean velocity and radial component of TKE. At the mean velocity field one can observe greater spreading rate of the jet and greater magnitude of $|\mathbf{U}|$ for $z/d > 0.7$ than for the isothermal jet. Also the centreline value reached negative value of almost –0.97 of U_0 that is about two times greater than for the isothermal flow. Thus, for the present case the presence of combustion increases intensity of the back flow in the recirculation zone that leads to the intensification of the vortex core precession (cf. values of $\langle v^2 \rangle$ near the nozzle exit in Figures 7c and 9c).

Photograph and CH* chemiluminescence image for the essentially different regime, namely lean swirling flame ($\Phi = 0.68$, $\mathrm{Re}_{air} = 6{,}800$, $U_0 = 7.2$ m/s) are shown in Figure 9a and b, respectively. For this regime, the flame front is considered to have a quasi-tubular shape in the initial region of the flame ($z/d < 1.5$). The image of chemiluminescence signal indicated that the shape of the flame front in not smooth, and a number of disturbances with a certain azimuthal mode is present on the flame surface.

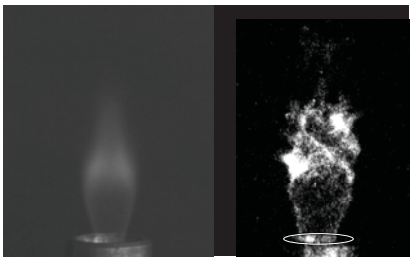

Figure 10. (a) Photograph and (b) CH* chemiluminescence image for a lean swirling flame at $\Phi = 0.68$, $\mathrm{Re}_{air} = 6{,}800$, $U_0 = 7.2$ m/s.

The instantaneous velocity field for this regime is presented in Figure 11a, where the flame front is schematically shown by a dashed line. One can observe, that the flow inside of the recirculation zone is almost laminar that is also reflected by the distribution of $\langle v^2 \rangle$, shown in Figure 11c. Besides, the back flow inside the recirculation zone is rather weak in comparison to the lifted swirling flame (see Figure 8) and the vortex core precession is almost absent. This can be explained by that the lean combustion regimes are usually characterised by a small heat release rate (also note a weak chemiluminescence of the lean flame) in contrast to combustion of near-stochiometric mixtures. From the instantaneous velocity field, one can observe that the vortices in the lean flame emerge as a dense chain propagating on the both sides of the quasi-tubular flame front and they are rather small in comparison to previous combustion case (the radial component of TKE is below than 0.11 of U_0^2). Thus, the weak precession of the vortex core and comparatively small size of the vortices, providing the mixing of the burnt gases with fresh mixture on the both sides of the flame front, must be responsible for the observed low level of the acoustic noise, namely 69 dB SLP ($\langle p^2 \rangle^{1/2}$ was below 0.06 Pa), emitted by the lean swirling flame.

The attempts of the low-amplitude acoustic forcing of the swirling flame at S = 1.0, preformed in the present study, gave no noticeable effect. However, as indicated in Alekseenko et al. (2008), periodical forcing with high amplitude can increase intensity of the turbulent fluctuations in the strongly swilling jet, and thus, can affect the swirling flame structure.

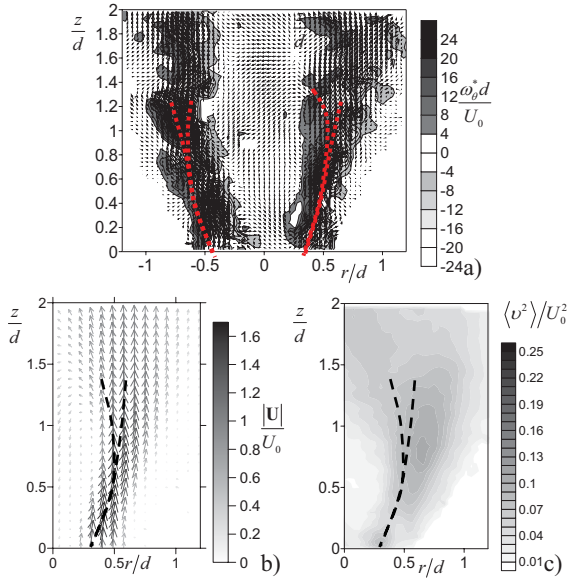

Figure 11. Spatial distribution of the (a) instantaneous velocity and vorticity, (b) mean velocity, (b) radial component of TKE for a lean swirling flame at Φ = 0.68, Re_{air} = 6,800, U_0 = 7.2 m/s.

CONCLUSIONS

A stereo PIV technique combined with a pressure probe and ICCD camera for CH* chemiluminescence measurement was applied for investigation of the large-scale vortices role in the turbulent structure of swirling premixed flames. For the investigated lifted combustion regimes, characterised by intensive acoustic fluctuations, interaction of the large-scale vortices, observed in the instantaneous velocity distributions, with the flame front is considered to be the major source of the intensive pressure fluctuations.

For the non-swirling lifted flame, the interaction of the ring-like vortices with the flame front was concluded to be responsible for the non-linear stabilisation mechanism of the premixed lifted flame via a pressure feed-back to the isothermal shear layer of the jet flow near the nozzle exit. This was indirectly confirmed by the effect of the additional acoustic forcing on the lifted flame structure.

For the swirling turbulent flames, intensive helical vortices were found to produce high-level turbulent fluctuations near the region of the flame front stabilisation. The combination of the back flow inside the recirculation zone, resulted from a vortex breakdown, and intensive turbulent heat and mass transfer due to the helical vortices is considered to be mainly responsible for the efficient stabilisation of a flame by applying a strong swirl.

ACKNOWLEDGEMENTS

This work was partially supported by RAS and SB RAS integration research projects and by the Russian Foundation for Basic Research (grants №№ 07-08-00213, 07-08-00710, 07-08-12254). The authors are grateful to Mikhail Tokarev for his assistance in processing of PIV images.

REFERENCES

Alekseenko, S.V., Kuibin, P.A., Okulov, V.L., 2007, *Theory of concentrated vortices: An Introduction*. Springer.

Alekseenko, S.V., Dulin, V.M., Kozorezov, Yu.S., Markovich, D.M., 2008, "Effect of axisymmetric forcing on the structure of a swirling turbulent jet", *Int. J. of Heat and Fluid Flow*, Vol. 29, pp. 1699-1715.

Billant, P., Chomaz, J.-M., Huerre, P., 1998, "Experimental study of vortex breakdown in swirling jets", *J. Fluid Mech.*, Vol. 376, pp. 183-219.

Coudert, S.J.M., Schon, J.-P., 2001, "Back-projection algorithm with misalignment corrections for 2D3C stereoscopic PIV", *Meas. Sci. Technol.*, Vol. 12, pp. 1371-1381.

Gallaire, F., Rott, S., Chomaz, J.-M., 2004, "Experimental study of a free and forced swirling jet", *Phys. Fluids*, Vol. 16, pp. 2907-2917.

Gupta, A.K., Lilley, D.G., Syred, N., 1984, *Swirl flows.* Abacus Press, Kent Engl.

Liang, H., Maxworthy, T., 2005, "An experimental investigation of swirling jets", *J. Fluid Mech.*, Vol. 525, pp. 115-159.

Lieuwen, T., Torres, H., Johnson, C., Zinn, B.T., 2001, "A mechanism of combustion instability in lean premixed gas turbine combustors", *J. Eng. Gas Turbines and Power*, Vol. 123, pp. 182-189.

Mourtazin, D., Cohen, J., 2007, "The effect of buoyancy on vortex breakdown in a swirling jet", *J. of Fluid Mech.*, Vol. 571, pp. 177-189.

Schneider, C., Dreizler, A., Janicka, J., 2005, "Fluid dynamical analysis of atmospheric reacting and isothermal swirling flows", *Flow, Turbul. Combust.*, Vol. 74, pp. 103-127.

Schuller, T., Durox, D., Candel, S., 2002, "Dynamics of and noise radiated by a perturbed impinging premixed jet flame", *Combust. and Flame*, Vol. 128, pp. 88-110.

Stella, A., Guj, G., Kompenhans, J., Raffel, M., Richard, H., 2001, "Application of particle image velocimetry to combusting flows: design considerations and uncertainty assessment", *Exp. Fluids*, Vol. 30, pp. 167-180.

Su, L.K., Han, D., Mungal, M.G., 2000, "Experimental results on the stabilization of lifted jet diffusion flames" *CTR Annual Research Briefs,* Center for Turbulence Research, Stanford University, pp. 79-89.

Treurniet, T.C., Nieuwstadt, F.T.M., Boersma, B.J., 2006, "Direct numerical simulation of homogeneous turbulence in combination with premixed combustion at low Mach number modelled by the G-equation", *J. Fluid Mech.*, Vol. 565, pp. 25-62.

Yoshida, H., Koda, M., Ooishi, Y., Kobayashi, K.P., Saito, M., 2001, "Super-mixing combustion enhanced by resonance between micro-shear layer and acoustic excitation", *Int. J. Heat and Fluid Flow*, Vol. 22, pp. 372-379.